J. Fluid Mech. (2004), *vol.* 510, *pp.* 105–129.
DOI: 10.1017/S0022112004009231 Printed in the United Kingdom

Active management of naturally separated flow over a solid surface. Part 1. The forced reattachment process

By A. DARABI AND I. WYGNANSKI

Department of Aerospace Engineering, University of Arizona, Tucson, AZ 85721, USA

(Received 20 April 2003 and in revised form 24 February 2004)

The forced reattachment of flow to an inclined flat surface, simulating a simple flap, was investigated experimentally. The transition from a separated to an attached state of the flow was initiated by an abrupt change in the frequency and the amplitude of periodic perturbations emanating from a slot at the flap shoulder. The excitation parameters determined the total duration of the reattachment process. Minimum reattachment time occurred at an optimal excitation frequency of $F^+_{opt} \approx 1.5$, which was independent of amplitude and flap inclination. The control over the process was achieved by enhancing large spanwise vortices in the flow. Spatial amplification of consecutive vortices induces mean transport of fluid away from the flap surface which causes the main stream to reattach. The time scales of the excitation are at least an order of magnitude smaller than the typical reattachment times.

1. Introduction

The efficacy of flaps and control surfaces on wings is limited by flow separation, thus, complex mechanical systems were devised to keep the flow attached. A typical flap on a commercial airliner is slotted, containing two or three moving elements that extend beyond the nominal trailing edge of the wing (Fowler flap). The 'part counts' of such flap systems run into thousands. Many of the subsystems and their actuators are heavy, expensive to build, and costly to maintain.

Flaps may be simplified or even entirely replaced by using periodic excitation to enhance lift and reduce drag on wings. Periodic excitation suppresses flow separation over the lifting surfaces (Seifert *et al.* 1993), thus enabling the attached flow to withstand a more severe adverse pressure gradient than would normally be possible in its absence (Seifert, Darabi & Wygnanski 1996; Greenblatt & Wygnanski 2001). The main advantage of this method of boundary-layer control stems from the amplification of the input disturbances by the pre-existent external flow. This unique feature of flow control makes it more difficult to understand, regardless of the ease of its implementation.

There are two initial states from which the control of separation could be approached. We may start with separated flow that has to be forced to reattach to the surface or we may excite the attached flow in order to delay its separation. Nishri & Wygnanski (1998, hereinafter referred to as NW) carried out a detailed parametric investigation of the various states of the flow above an inclined flat plate (a generic flap) subjected to periodic excitation. The upstream boundary layer in their experiment was fully turbulent and two-dimensional. The separation line was well defined, coinciding always with the location of the actuation, and the solid surface

was never too far removed from the separation-streamline. The experiment allowed controlled transitions between separated and attached states by altering the excitation amplitude or its frequency. It was demonstrated that periodic excitation at a prescribed frequency can force a separated flow to reattach, provided that a threshold amplitude is exceeded. This threshold depends on the flap deflection, on its length, and on some details of its design (e.g. the height of the gap). Once the flow reattached, it would not separate again even when the amplitude was reduced below the above-mentioned threshold, or the frequency was changed within some prescribed limits. The process demonstrated hysteresis with respect to the forcing parameters.

Some investigators, who used periodic excitation to improve the performance of their flow systems, did not consider the location of the actuation relative to the natural separation location as being important, nor did they report the upstream flow conditions or the initial state of the flow (i.e. whether it was attached or separated). The curvature of the surface, which greatly affects the level of excitation that is required to maintain the flow attached, was also hardly considered (Greenblatt & Wygnanski 2001). These factors, combined with the complex issues of hysteresis led to misinterpretations of data and to possible confusion. Most of the present controversy surrounds the choice of the dimensionless frequency F^+, applied to reattach separated flow ($F^+ = fx/U_\infty$ where f is the excitation frequency, U_∞ is the free-stream velocity and x is the distance between the actuation and the trailing edge of the flap or the airfoil). The resolution of this controversy is important, since frequency is the primary parameter determining the effectiveness of the excitation.

A typical dimensionless frequency associated with the roll-up of the separated shear layer into discrete vortices (often referred to as vortex shedding), when based on the wake width δ, and the free-stream velocity is of order $S_{t\delta} = f\delta/U_\infty \approx 0.18$. In the case of a circular cylinder, the width of the near wake is approximately equal to the diameter of the cylinder and, therefore, the two are often interchanged ($S_{t\delta} \approx S_{tD}$). The Strouhal number is proportional to the ratio of two characteristic length scales: the wake width and the wavelength associated with the periodic vortex roll-up. The latter may be 3 to 6 times larger than the diameter of the cylinder at high Re (because the phase velocity in the near wake is approximately 1/2 of the free-stream velocity). Since the most effective periodic excitation used to delay separation on a circular cylinder (Béra *et al.* 2000; Taubert, Kjellgren & Wygnanski 2002), has a wavelength comparable to its radius, the excitation frequencies are an order of magnitude higher than the vortex-shedding frequency.

On thin airfoils, characterized by a leading-edge stall at small angles of incidence, the width of the wake is typically commensurate with the projected length that is orthogonal to the free stream (i.e. $c \sin\alpha$ where c is the chord of the airfoil). At a typical incidence angle, $\alpha \approx 12^\circ$, this renders $S_{tc} = fc/U_\infty \approx 1$. If the actuation is applied to the airfoil leading edge, resulting in an attached flow over the entire upper surface, then the most effective dimensionless frequency of excitation is $F^+ = f_e c/U_\infty \approx S_{tc} = 1$. If on the other hand, we consider a flapped wing of a tilt rotor airplane in hover (i.e. $\alpha \approx -90^\circ$; see e.g. Grife, Darabi & Wygnanski 2002), where the actuators are located at the flap shoulder, the optimum frequency of excitation might again be an order of magnitude higher than the shedding frequency.

On thin airfoils at $Re < 10^6$, laminar separation may be followed by transition that leads to turbulent reattachment, whereas on bluff bodies, such as the circular cylinder, the solid boundary recedes from the separated shear layer, limiting the opportunity for subsequent reattachment. Periodic excitation introduced into the laminar boundary layer acts as a trip that accelerates the transition to turbulence,

resulting in a delay of separation that evokes a drag crisis on bluff bodies (i.e. a drastic reduction in drag). In this case, the actuation should be located considerably upstream of the natural separation location and the frequencies of excitation should correspond to the most receptive frequencies of the boundary layer. The dominant frequencies triggering transition may be two orders of magnitude higher than the vortex-shedding frequencies (Ahmed & Wagner 2003) and are an order of magnitude higher than the most effective frequencies responsible directly for the delay of separation (Naim 2003). The indirect process of separation control that invokes transition to turbulence was envisaged by Collins & Zelenevitz (1975). It has most probably dominated the flow of Amitay, Smith & Glezer (1998) who equated transition with 'aerodynamic shaping'.

Sometimes, the natural separation location might be far upstream of the actuation. This usually happens on deeply stalled airfoils with highly deflected flaps (Greenblatt & Wygnanski 2001). In this case, periodic excitation might affect the upstream flow, in spite of the fact that reattachment downstream of the actuator is not attained. We should probably refer to these cases as management of separated flow rather than control of separation. We could reason that such management will require high amplitudes and low frequencies (large eddies) in order to interact with a distant mixing layer and change its orientation relative to the free stream.

Controversies about the optimal frequencies of excitation flourished because the purpose of this excitation was unclear. Should it maintain attached flow in spite of the severe adverse pressure gradient or should it force reattachment of an already separated flow and help in the pressure recovery. It seemed that a better understanding of the flow dynamics during the process of separation or reattachment would provide the reason for the best choice of excitation frequency. Nishri (1995) made some preliminary observations of the time-dependent effects associated with changes in the actuation that led either to separation or reattachment of the flow. He reported that the transient time scales were totally different from those associated with the excitation and this warranted further investigation.

The practical significance of the time-dependent phenomena may be appreciated when we consider possible uses of flow control by periodic excitation. Replacement of conventional control surfaces (e.g. rudders, elevators or ailerons) and alleviation of atmospheric turbulence through a closed-loop control approach are but two examples of potential applications. Clearly, developing the technology requires familiarity with the transient behaviour of flow that is subjected to periodic perturbation.

The present experiment aimed at a better understanding of the temporal response of the flow to a variety of changes in the actuation. It was conducted on a generic flap configuration where only stepwise changes in the excitation were used to force reattachment of the flow to the stalled flap. Changes in excitation resulting in a controlled separation of the flow from the surface will be discussed separately. The flow in this experiment was incompressible and the Reynolds number based on the flap length (Re_L) was less than 5×10^5.

2. The experiment

2.1. *Apparatus and data acquisition*

The experiment was carried out in a cascade wind tunnel described by Oster & Wygnanski (1982), Katz, Nishri & Wygnanski (1989) and NW. A straight Plexiglas flap of chord $L_f = 240\,\text{mm}$ was hinged to the test-section sidewalls at the edge of a much longer horizontal flat plate. A 2 mm high nozzle formed between the horizontal plate and the flap hinge allowed introduction of periodic perturbations into the flow.

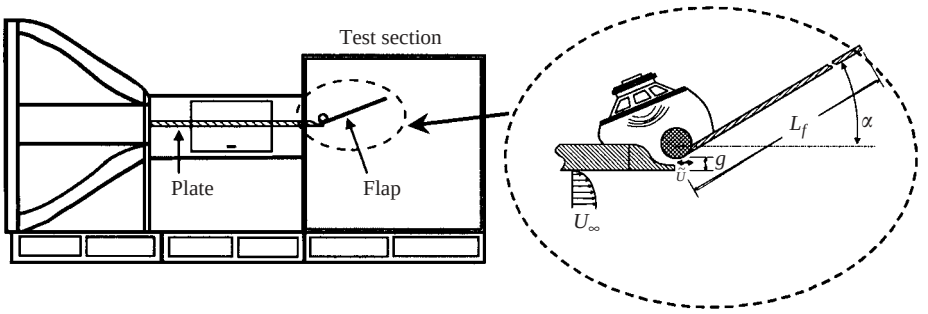

FIGURE 1. Schematics of the test section and the flap geometry.

The transparent Plexiglas sidewalls maintained the two-dimensional flow and enabled DPIV (digital particle image velocimetry) imaging. The flow over the horizontal upstream plate was tripped by distributed roughness (see NW). The test section and the flap are shown in figure 1.

Periodic flow perturbations were generated by a woofer situated in a sealed chamber behind the flap (figure 1). The amplitudes of the excitation were determined for each input voltage and frequency of interest by using a single hot-wire probe positioned at the nozzle exit. To avoid signal rectification, measurements were made in the presence of a constant outward airflow. The results were used to calculate the oscillatory momentum coefficient, $\langle c\mu \rangle = \langle u_j \rangle^2 b/0.5 U_\infty^2 L_f$ (where $\langle u_j \rangle$ is the phase-locked and ensemble-averaged amplitude of the excitation velocity at the slot whose width is b), after the two-dimensionality and the uniformity of the velocity profiles near the nozzle were verified. Two signal generators and a specially fabricated timing device were used to switch abruptly between different sustained excitation settings. This caused the flow to either separate or reattach to the flap surface, depending on the end values of frequency and amplitude selected.

A multi-channel array of differential pressure transducers (± 20 mm H_20 full-scale) was used to measure the dynamic distributions of surface pressure along the flap's chord. The pressure was read simultaneously at a rate of 2.4 kHz per channel through twenty pressure taps that were unevenly distributed along the centreline of the flap. Since the transducers were not embedded in the surface, the frequency-dependent attenuation of the pressure signals and their phase shift was calibrated. This allowed restoration of the actual amplitude and phase of the coherent surface-pressure fluctuations at each tap.

A two-dimensional PIV (made by IDT) was used to measure the velocity field in a plane that was parallel to the flow and perpendicular to the flap surface (at mid-span). The flow was seeded far upstream of the test section by polydispersed (0.1–10 μm) fog particles commonly used in theatres. The camera (Kodak AE-1.0) featured a double-exposure mode and had a resolution of 1016×1016 at 8-bit. Because of the limited power of the laser (Dual Nd:YAG by Spectra-Physics), the effective light sheet, and the PIV field-of-view, spanned only about 60% of the flap chord. The results are presented in a coordinate system that is parallel and normal to the flap surface with its origin located at the slot exit. In order to estimate the accuracy of the PIV data, several cases were compared to hot-wire measurements at the same conditions. The discrepancy between the two data sets in the absence of reverse flow was never greater than 5%.

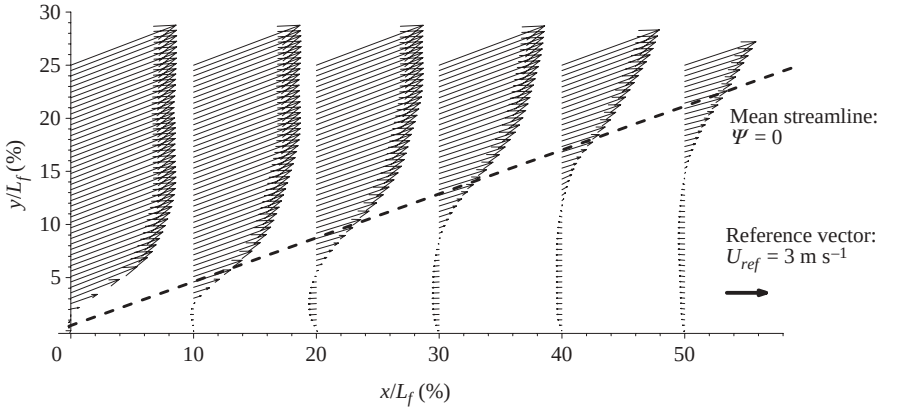

FIGURE 2. The separated baseline flow; $Re_L = 1.24 \times 10^5$, $\Delta\alpha_r = 6^\circ$, $F^+ = \langle c\mu \rangle = 0$.

Both mean and phase-locked pressure and velocity measurements were acquired by ensemble averaging some 150 events (flow realizations) for different times and flow situations. Mean quantities were obtained by capturing events at $t > 0$ when the abrupt change in the excitation at $t = 0$ was not synchronized with its phase (i.e. phase was random at the instance of measurement). Phase-locked data were acquired by synchronizing changes made in the excitation at $t = 0$. In those cases, the timing of the measurements explicitly determined their phase.

2.2. *The uncontrolled base flow*

The condition of the unperturbed (baseline) flow over the inclined flap is a function of the deflection angle α and the height of the discontinuity G at the flap hinge (i.e. the slot width and the thickness of the upper slot lip (figure 1). At relatively small deflections, the flow is attached to the flap. It develops minimum static pressure just above the hinge after accelerating over the upstream horizontal surface. Owing to the sharp discontinuity at the knee, a turbulent separation bubble is created over the fore part of the flap whose size is dependent on the flap deflection. Flow separation occurs when α is increased beyond the natural separation angle, α_{s0}, that causes the bubble to burst. In the present case, this angle was $\alpha_{s0} \approx 18^\circ$.

In order to enforce reattachment of the flow, the deflection angle has to be decreased back to an angle α_{r0} – the natural reattachment angle – which is always smaller than α_{s0} (implying the existence of hysteresis with respect to α). Both α_{s0} and α_{r0} are very sensitive to the details of the flap shoulder geometry, but almost independent of the upstream boundary-layer thickness and the global Reynolds number Re_L (NW).

Figure 2 illustrates PIV measurement of the mean velocity field, when the base flow was separated at an excessive flap angle of $\Delta\alpha_r = \alpha - \alpha_{r0} = 6^\circ$. The flow is represented by profiles of velocity vectors extracted from the PIV data at several cross-sections along the flap. A dashed line in the figure represents the position of the mean separation streamline ($\psi = 0$). Since there is no pressure gradient normal to this streamline, it does not curve, but rather preserves the original flow inclination of $\alpha = 23^\circ$ relative to the flap. The separation streamline and the flap surface define a re-circulation (or a 'dead water') zone that accommodates weak reverse flow velocities that are smaller than $0.1U_\infty$. In this case the velocity ratio parameter, $R = (U_{max} - U_{min})/(U_{max} + U_{min})$ is larger than unity ($R_{max} \sim 1.2$), implying a potential

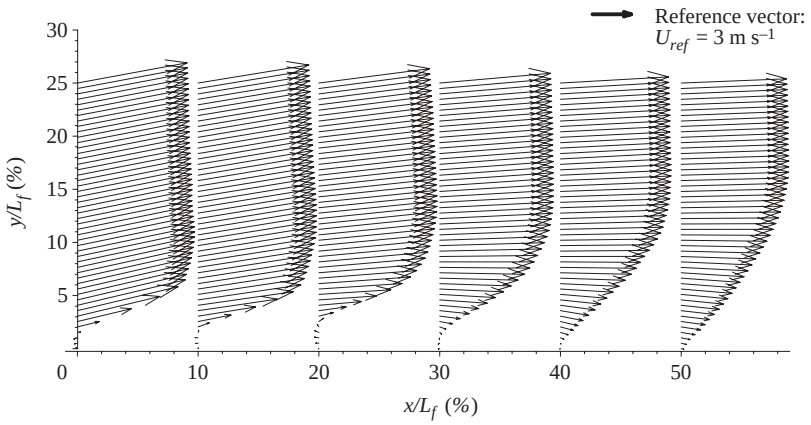

FIGURE 3. The forcefully attached flow; $Re_L = 1.24 \times 10^5$, $\Delta\alpha_r = 6^\circ$, $F^+ = 1.2$, $\langle c\mu \rangle = 0.02\%$.

for strong spatial amplification of convective disturbances in the separated shear layer (Huerre & Monkewitz 1990).

2.3. *The steady-state controlled flow*

Starting with a detached basic state, application of oscillatory control may force reattachment of the flow to the surface, depending on the specific excitation parameters used. Using optimal reduced frequency of $F^+_{opt} \approx 1.2$ maximizes the attainable attached deflection angle $\Delta\alpha_r = \alpha_r - \alpha_{ro}$ and the normal force coefficient C_n, when $\langle c\mu \rangle$ is prescribed. Figure 3 represents a sample of the mean attached flow above the flap that was forced at $F^+ = 1.2$ and $\langle c\mu \rangle = 0.02\%$, when the deflection angle in excess of natural reattachment was $\Delta\alpha_r = 6^\circ$. The figure reveals the existence of a constant elongated recirculation zone that spans about 45% of the flap chord and has a maximum height of $y/L_f \approx 4\%$. The time-mean reverse velocities in the bubble do not exceed $\bar{u}/U_\infty \approx 5\%$.

2.4. *The transition between attached and separated flow*

Three dominant variables, α, F^+ and $\langle c\mu \rangle$ determine whether the flow is attached to or separated from a flap of a given length. The two domains in the parameter space $\{\Delta\alpha, F^+, \langle c\mu \rangle\}_r$ and $\{\Delta\alpha, F^+, \langle c\mu \rangle\}_s$, representing attached and separated states, respectively, overlap one another, implying that either state can be maintained by the same controlling parameters depending on the initial condition. Forced separation and reattachment of the flow at constant $\alpha > \alpha_{r0}$ is obtained by changing parameter values between $\{F^+, \langle c\mu \rangle\}_r$ and $\{F^+, \langle c\mu \rangle\}_s$ in an abrupt manner. In the present investigation, only step changes in actuation parameters that cause the flow to reattach were considered. The process of flow separation is discussed in Part 2 (Darabi & Wygnanski 2004).

3. The process of flow reattachment

3.1. *The mean flow*

Starting with unforced separated flow at constant $\alpha > \alpha_{r0}$, reattachment is caused by initiation of excitation with sufficient control authority $\{F^+, \langle c\mu \rangle\}_r$. Figure 4 illustrates the changes in the mean normal force coefficient, $C_n = N/0.5\rho U_\infty^2 L_f$ (where N is the normal aerodynamic force per unit span and ρ is the air density), experienced

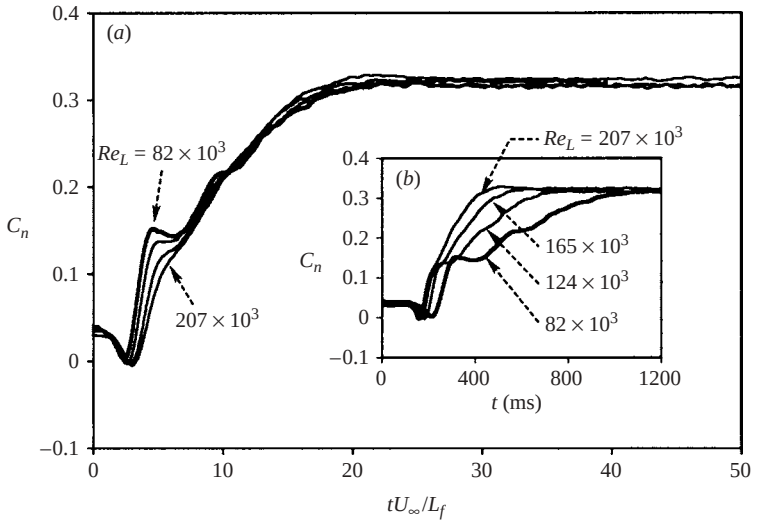

FIGURE 4. The effect of Re_L and time normalization on the evolution of C_n during reattachment; $\Delta\alpha_r = 6°$, $F^+ = 2.4$, $\langle c\mu \rangle = 0.05\%$.

by the flap during the reattachment process at several Reynolds numbers ranging from 8.2×10^4 to 20.7×10^4. The flap deflection ($\Delta\alpha_r = 6°$), the reduced frequency ($F^+ = 2.4$) and the amplitude ($\langle c\mu \rangle = 0.05\%$) were all maintained at a constant level during the reattachment process. The results scale with a dimensionless time $\tau = tU_\infty/L_f$ (cf. figures 4*a* and 4*b*).

During the initial stages of reattachment, a decrease in C_n is noted, reaching a minimum between $\tau = 2.5$ and $\tau = 3$, depending on Re_L. This minimum is followed by an abrupt increase in the normal force that terminates before $\tau \approx 6$ (with a sharp discontinuity at low Re_L). Thereafter, C_n increases almost linearly with τ until the process nears its completion and a steady flap loading is established. The dimensionless time required to complete the reattachment process was practically independent of Re_L under the tested conditions and provided the justification for the proposed scaling.

The changes in flap loading during reattachment under a variety of forcing conditions are plotted in figure 5. Three different frequencies $F^+ = 0.64$, 1.92 and 2.52 were applied at amplitudes ranging from $\langle c\mu \rangle = 0.02\%$ to $\langle c\mu \rangle = 0.08\%$, while keeping $\Delta\alpha_r = 6°$ and $Re_L = 1.65 \times 10^5$. It is evident that at a constant Re_L, the initial transient drop in flap loading is almost independent of the excitation used. Both the time corresponding to a minimum C_n and its subsequent steep recovery at $2.5 \lesssim \tau \lesssim 5$ are not affected by F^+. Increasing $\langle c\mu \rangle$ does not change the time of occurrence of the minimum C_n, but it causes $C_{n,min}$ to fall further below its separated value. Values of $|C_{n,min} - C_{n0}| > 0.075$ are observed when $\langle c\mu \rangle = 0.08\%$ and they are roughly proportional to $\langle c\mu \rangle$. Beyond $\tau \approx 5$, the increase in flap loading is typically linear with time, with the exception of the lowest excitation frequency ($F^+ = 0.64$). Clearly, the duration of the reattachment process increases dramatically when the flow is excited inadequately, particularly when the amplitudes are too low (figure 5). On the other hand, there is a minimum time limit for the completion of the process.

The total dimensionless time required for reattachment, τ_r, was defined by letting the maximum slope of $(\mathrm{d}C_n/\mathrm{d}\tau)_{max}$ intersect the extension of the final steady-state value of C_n (figure 6). Although not always accurate (particularly at low frequencies,

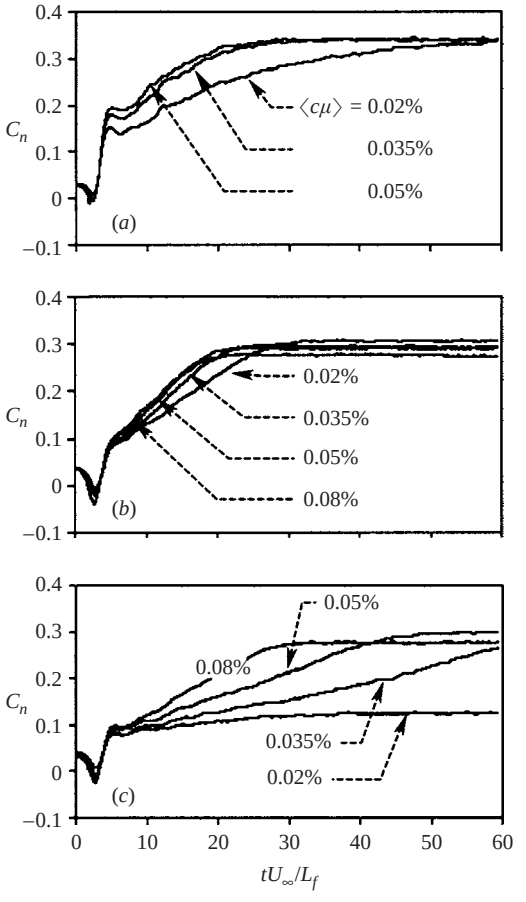

FIGURE 5. The effect of the forcing parameters on the evolution of C_n during reattachment; $\Delta\alpha_r = 6°$, $Re_L = 1.65 \times 10^5$. (*a*) $F^+ = 0.64$; (*b*) 1.92; (*c*) 2.52.

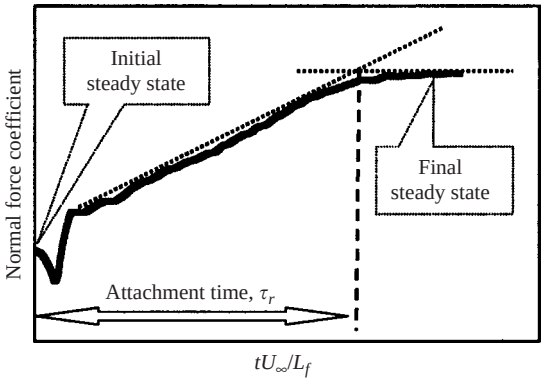

FIGURE 6. The definition of τ_r.

where there is no obvious linear stage), the values of τ_r adequately reflect the efficacy of the excitation. Plotting the dependence of τ_r on F^+ for various levels of $\langle c\mu \rangle$, at constant $\Delta\alpha_r = 6°$ (figure 7), accentuates the existence of a minimum duration required for reattachment. Apparent saturation, with respect to amplitudes beyond

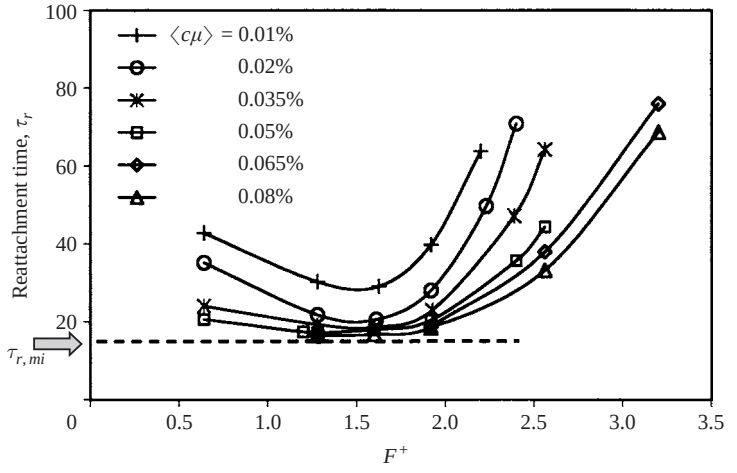

FIGURE 7. The reattachment time τ_r as a function of F^+ for different $\langle c\mu \rangle$; $\Delta\alpha_r = 6°$, $Re_L = 1.24 \times 10^5$.

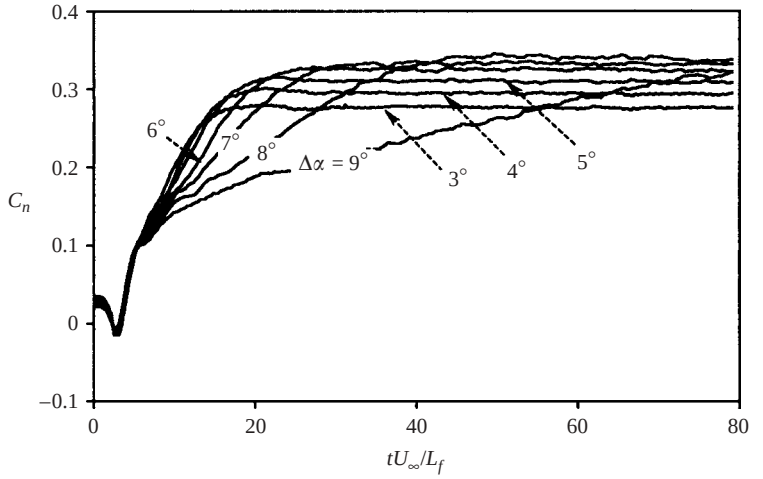

FIGURE 8. The effect of $\Delta\alpha_r$ on the evolution of C_n during reattachment; $Re_L = 1.24 \times 10^5$, $F^+ = 1.2$, $\langle c\mu \rangle = 0.05\%$.

$\langle c\mu \rangle = 0.08\%$, suggests that, for the assigned flap deflection, a minimum reattachment time is approximately $\tau_{r,min} = 16$. The minimum reattachment time is clearly associated with an optimum reduced frequency of $F^+_{opt} \approx 1.5$, which is not sensitive to the input amplitude. Below and beyond F^+_{opt}, reattachment time increases at a rate that depends on $\langle c\mu \rangle$. Note that the similarity between the dependence of τ_r on F^+ and the dependence of the minimum amplitude required for reattachment on F^+ suggests that the frequency resulting in the quickest reattachment is also the most efficient one (see NW).

Figure 8 illustrates the effect of changing $\Delta\alpha_r$ on C_n when the flow is forced to reattach at constant values of $F^+ = 1.2$ and $\langle c\mu \rangle = 0.05\%$. An increase in the deflection angle at a constant F^+ and $\langle c\mu \rangle$ concomitantly increases the time required for reattachment until a threshold value of $\Delta\alpha_r$ is reached at which the flow can no

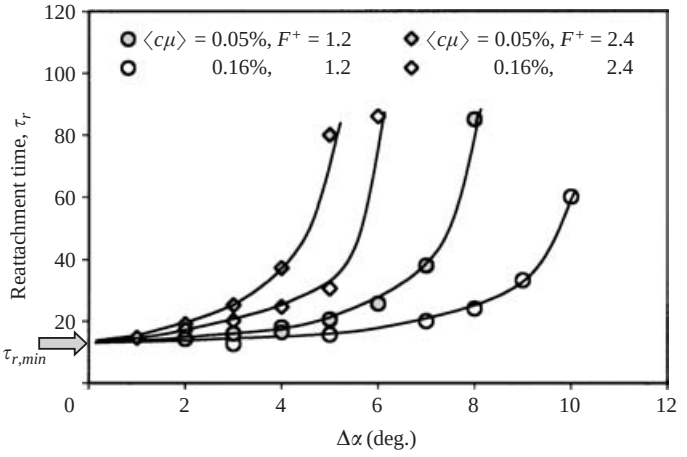

FIGURE 9. The effect of $\Delta\alpha_r$ on the reattachment time for different excitation conditions.

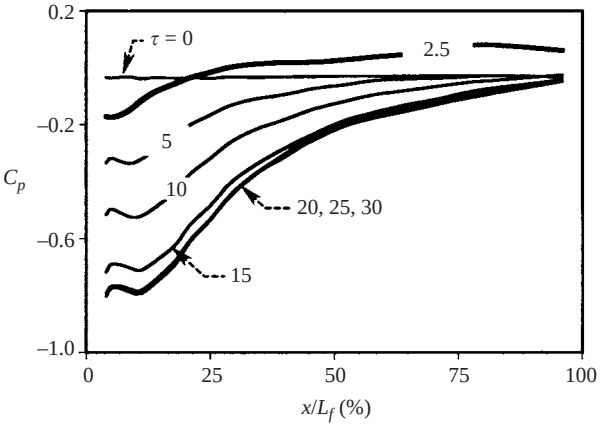

FIGURE 10. Spatial distribution of the mean C_p during reattachment; $Re_L = 1.24 \times 10^5$, $\Delta\alpha_r = 6°$, $F^+ = 1.28$, $\langle c\mu \rangle = 0.05\%$.

longer reattach to the surface at the prescribed excitation (figure 9). The dip in C_n during the initial stages of reattachment is again not affected by $\Delta\alpha_r$.

Figure 10 describes variations in the streamwise distribution of the pressure coefficient, C_p, during reattachment using excitation at $F^+ = 1.28$ and $\langle c\mu \rangle = 0.05\%$, when the excessive flap deflection was $\Delta\alpha_r = 6°$. The bolder line, describing the C_p at $\tau = 2.5$, shows that the initial offloading of the flap is a result of positive pressures that extend over large aft portions of the flap. For $\tau > 5$, C_p decreases almost everywhere, at a rate that depends on the location along the flap and the effectiveness of the forcing. The final steady-state pressure levels are typically attained first near the trailing edge, where the total velocity changes are small. When the same results are cross-plotted against τ (figure 11), the initial adverse surge in flap loading is manifested by a single positive ripple in the local mean wall pressures, which progressively moves downstream with increasing time. The amplitude of this excursion in C_p increases with x and with time, reaching a maximum value around $x/L_f = 80\%$ at $\tau \approx 2.5$. Since roughly the same period is required for the C_p at a given pressure tap to return

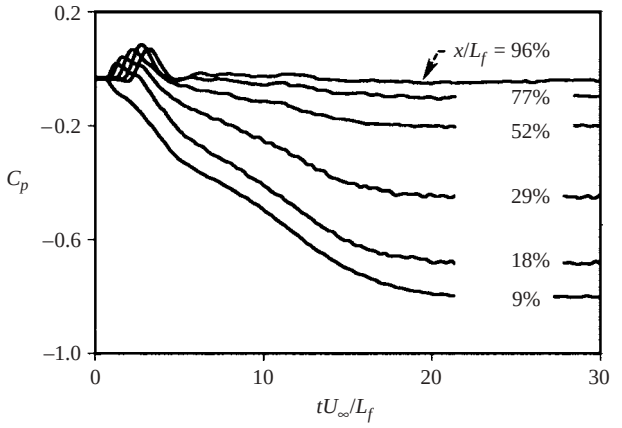

FIGURE 11. Temporal evolution of the mean C_p during reattachment; $Re_L = 1.24 \times 10^5$, $\Delta\alpha_r = 6^\circ$, $F^+ = 1.28$, $\langle c\mu \rangle = 0.05\%$.

to its original value, the offloading of the flap does not vanish until the recovery at the furthest x-location has been completed at $\tau \approx 5$.

Changes in the mean velocity field during the reattachment process are exemplified by six mean PIV measurements, taken at sequential time steps, in figure 12. The flow was forced at $F^+ = 1.1$ and $\langle c\mu \rangle = 0.06\%$ when the excess deflection angle was $\Delta\alpha_r = 9^\circ$. The various shades of grey in the figure represent isodynes (constant contours of the spanwise vorticity). They are overlaid by uniformly spaced streamlines. The time intervals between adjacent figures are smaller during the initial transient in order to elucidate the rapid changes occurring in the flow at this stage.

It is apparent that during the first forcing cycle of the excitation (figure 12*b*), the imposed perturbation has not propagated far downstream, leaving the separated shear layer still intact beyond $x/L_f \approx 35\%$. Upstream of this point, a new recirculation zone is formed, marked in figure 12(*b*) by a closed streamline centred around $x/L_f \approx 12\%$. Between these two points, a region of diverging streamlines indicates local deceleration of the flow near the surface. These observations are substantiated by considering profiles of the streamwise velocity component $\bar{u}/U_\infty$ (figure 13), extracted from the PIV results at $x/L_f = 28\%$ and at various times τ. The pre-existing weak reverse flow at this x-location disappeared by the end of the first forcing cycle ($\tau = 0.9$) whereupon the local streamlines converged toward the surface in order to reappear with a renewed strength soon thereafter.

In subsequent time steps, the recirculation region intensifies and expands in the streamwise direction until at $\tau = 1.8$ it covers about half of the flap chord (figure 12*c*). Sometime between $\tau = 3.6$ and $\tau = 7.2$ the recirculation zone is swept away beyond the flap trailing edge. The similarity between the time required to build up the initial recirculation zone and the duration of the initial offloading of the flap, indicates that the two events are correlated. The remaining portion of the reattachment process is characterized by the steady approach of the shear layer to the surface, which, at the end of the process, encloses a thin elongated bubble over the fore part of the flap (figure 12*f*).

The velocity profiles plotted in figure 13 reveal the possibility that the velocity ratio parameter, $R = (U_{max} - U_{min})/(U_{max} + U_{min})$, exceeds the critical value necessary to make the flow globally unstable. This ratio is $R = 1.31$ for a mixing layer between two parallel streams and it has been exceeded over the front portion of the flap during

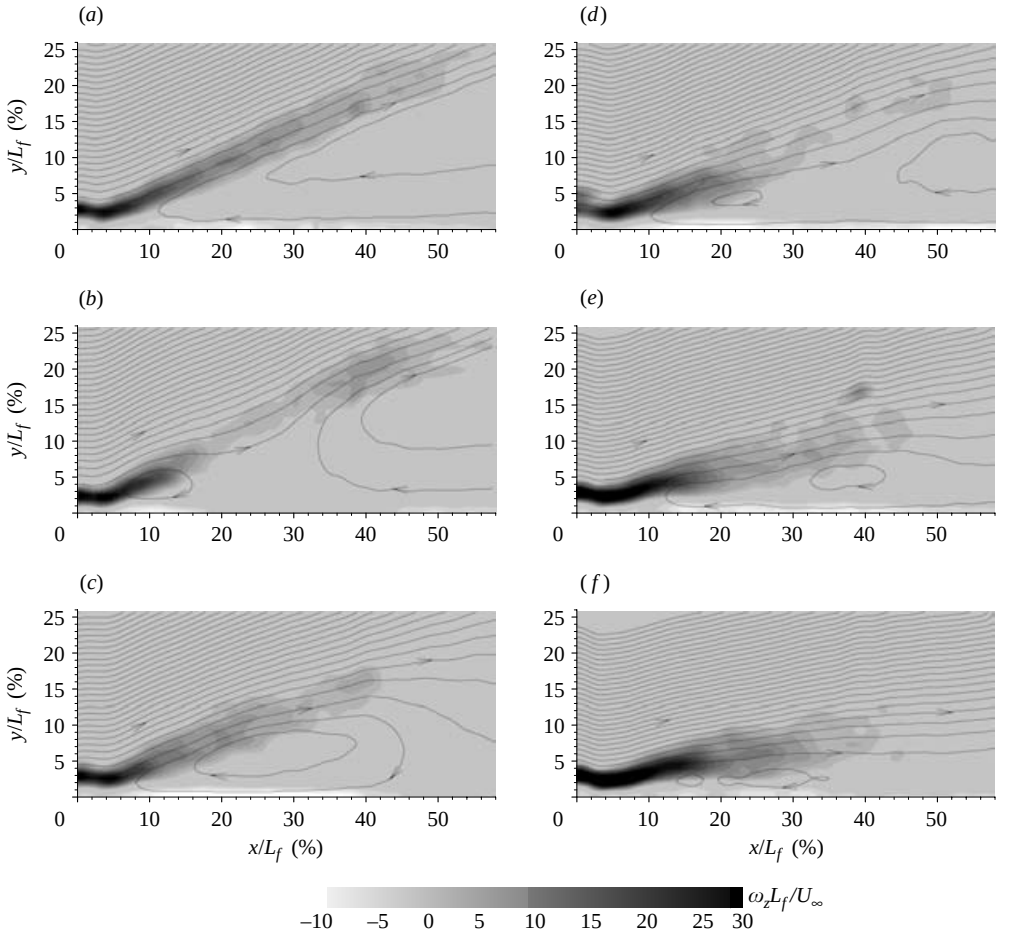

FIGURE 12. Mean vorticity and streamlines during reattachment; $Re_L = 1.44 \times 10^5$, $\Delta\alpha_r = 9°$, $F^+ = 1.1$, $\langle c\mu \rangle = 0.06\%$. (*a*) $\tau = 0$. $t = 0$ ms. (*b*) $\tau = 0.9$, $t = 25$ ms. (*c*) $\tau = 1.8$, $t = 50$ ms. (*d*) $\tau = 3.6$, $t = 100$ ms. (*e*) $\tau = 7.2$, $t = 200$ ms. (*f*) $\tau = 28.8$, $t = 800$ ms.

the initial time period of $1 < \tau < 5$, possibly resulting in a locally absolutely unstable flow.

3.2. *Phase-locked quantities*

The phase-locked pressure coefficients $\langle C_p \rangle$ measured during the reattachment process are shown in figure 14 for some selected pressure taps along the flap. Of the numerous excitation frequencies considered, only one case ($F^+ = 1.28$) is plotted for illustration. As might have been expected, the phase-locked pressures over the entire surface of the flap are oscillatory, reflecting imprints of the passing structures generated by the excitation. Close to the leading edge ($x/L_f < \sim 50\%$) and throughout most of the reattachment process, each passage of a vortex is associated with an incremental decrease in the local mean pressure. The magnitude of the change is not constant along the flap and it depends on F^+ and on $\langle c\mu \rangle$. The apparent spatial growth and subsequent decay of the wall pressure amplitudes is discussed in § 3.3.

The two fundamental time scales associated with forced reattachment, namely, the period of the oscillations (25 ms) and the time necessary for the completion

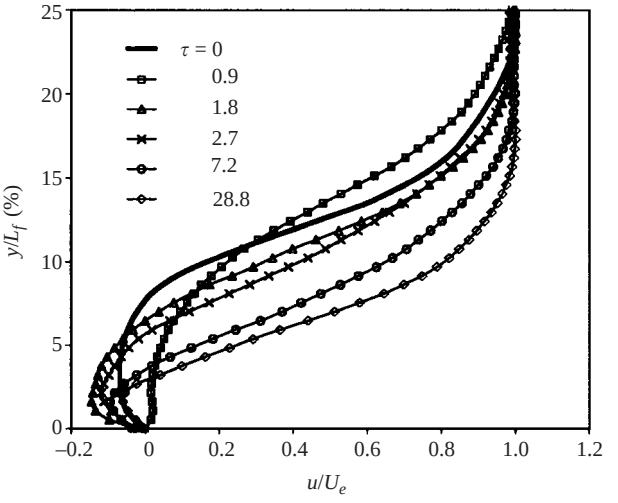

FIGURE 13. Normalized mean velocity profiles during reattachment at $x/L_f = 28\%$; $Re_L = 1.44 \times 10^5$, $\Delta\alpha_r = 9°$, $F^+ = 1.1$, $\langle c\mu \rangle = 0.06\%$.

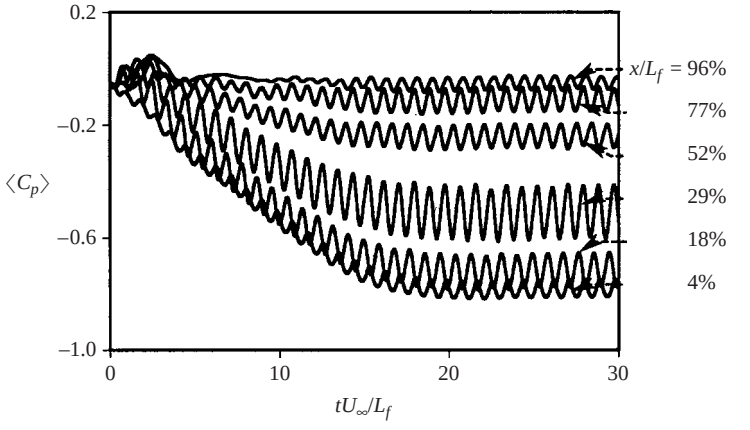

FIGURE 14. Temporal evolution of $\langle C_p \rangle$ at various streamwise locations along the flap; $Re_L = 1.24 \times 10^5$, $\Delta\alpha_r = 6°$, $F^+ = 1.28$, $\langle c\mu \rangle = 0.05\%$.

of the process, are clearly distinguishable in figure 14. The ratio between the two time scales, signifying the number of forcing cycles $N_r = f t_r = F^+ \tau_r$ occurring during the process, decreases monotonically with decreasing F^+. The value of N_r becomes almost independent of $\langle c\mu \rangle$ around $F^+ = 1.5$ (figure 15), but it is very sensitive to $\Delta\alpha_r$, particularly at high deflection angles (not shown). Although there is no apparent optimum for the number of cycles required for reattachment, extrapolating the dependence of N_r on F^+ to the ordinate yields $N_{r,min} \approx 10$. This demonstrates that there is at least an order of magnitude difference between the time scale of excitation and the time required for reattachment.

The phase-locked velocities during reattachment were measured using PIV under conditions identical to those shown in figure 12. Figure 16 represents six time steps measured at intervals of 1/4 period during the initial two cycles of the perturbation ($\tau \leqslant 1.81$). Data acquired at later times, but at the same phase relative to the excitation

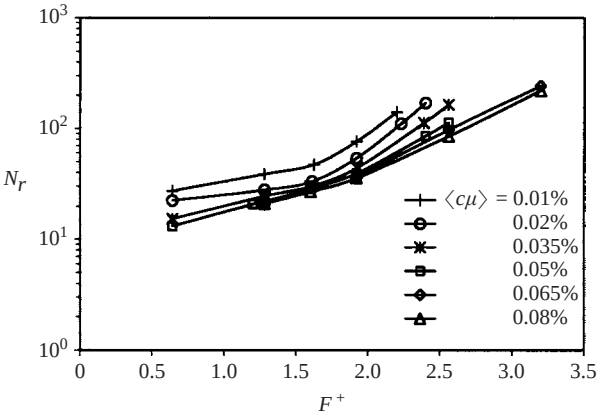

FIGURE 15. Influence of F^+ and $\langle c\mu \rangle$ on the number of cycles prior to reattachment, N_r.

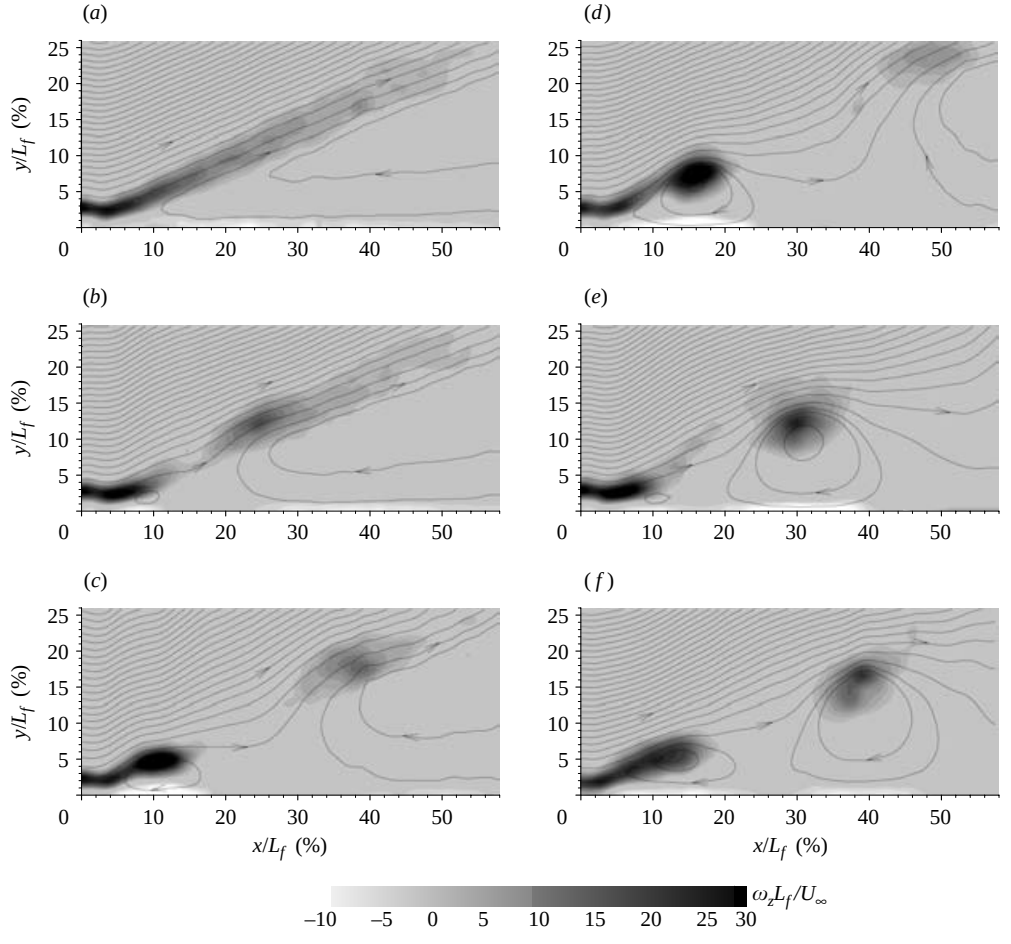

FIGURE 16. Phase-locked vorticity and streamlines during early reattachment (the first two forcing cycles); $Re_L = 1.44 \times 10^5$, $\Delta\alpha_r = 9°$, $F^+ = 1.1$, $\langle c\mu \rangle = 0.06\%$. (*a*) $\tau = 0$, $t = 0$ ms. (*b*) $\tau = 0.68$, $t = 18.75$ ms. (*c*) $\tau = 0.90$, $t = 25$ ms. (*d*) $\tau = 1.13$, $t = 31.25$ ms. (*e*) $\tau = 1.58$, $t = 43.75$ ms. (*f*) $\tau = 1.81$, $t = 50.0$ ms.

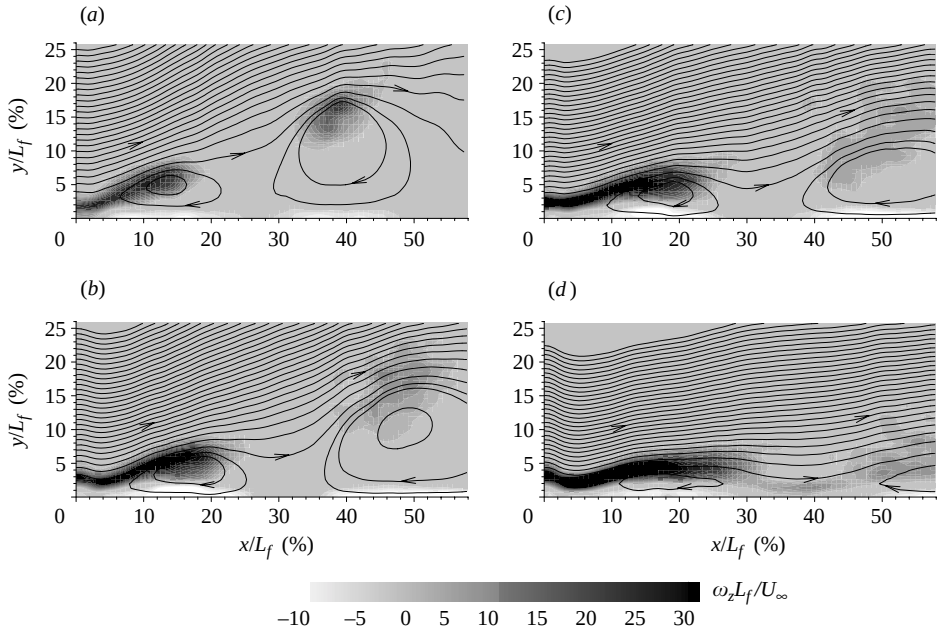

FIGURE 17. Phase-locked vorticity and streamlines during reattachment at equal phase relative to the excitation (long term); $Re_L = 1.44 \times 10^5$, $\Delta\alpha_r = 9°$, $F^+ = 1.1$, $\langle c\mu \rangle = 0.06\%$. (*a*) $\tau = 1.8$, $t = 50$ ms. (*b*) $\tau = 5.4$, $t = 150$ ms. (*c*) $\tau = 10.8$, $t = 300$ ms. (*d*) $\tau = 28.8$, $t = 800$ ms.

signal, are shown in figure 17. As before, the results are presented in the form of vorticity contours overlaid by streamlines.

The initiation of actuation fragments the uniform clockwise circulation stretching over the entire length of the flap by concentrating the vorticity near the flap hinge and rolling it into a small vortex (figure 16*b*). As this vortex propagates downstream and intensifies, fluid particles just in front (downstream) of it are slowed down and redirected toward the surface. This is manifested by streamline divergence (and hence a pressure increase) seen downstream of the vortex (figure 16*b*, *c*). During the second forcing cycle (figure 16*d*–*f*), the first vortex separates from the continuous vorticity sheet near the flap shoulder and it propagates downstream and away from the wall, intensifying the high-pressure region. This effect becomes weaker during the third and fourth cycles and is subsequently negligible. As time progresses (figure 17), the detached vortex lump that is so obvious during the second cycle of excitation appears to become more diffuse while progressively approaching the surface at each passing cycle. By the end of the process, the phase-averaged streamlines are almost parallel to the surface (figure 17*d*). Mapping the trajectories of the vortex lumps during the second, sixth and twelfth cycles after the initiation of excitation (figure 18) indicates that the average vortex approaches the surface faster during the earlier part of the process (second to sixth cycle). It also reveals an increase in the advection speed of the vortices with time (see below).

3.3. *Some characteristics of the coherent motion*

The inadequate temporal resolution of the available PIV data made it impractical to assess the evolution of the coherent eddies in the time domain. However, the apparent correlation between the ensemble-averaged eddies observed and the

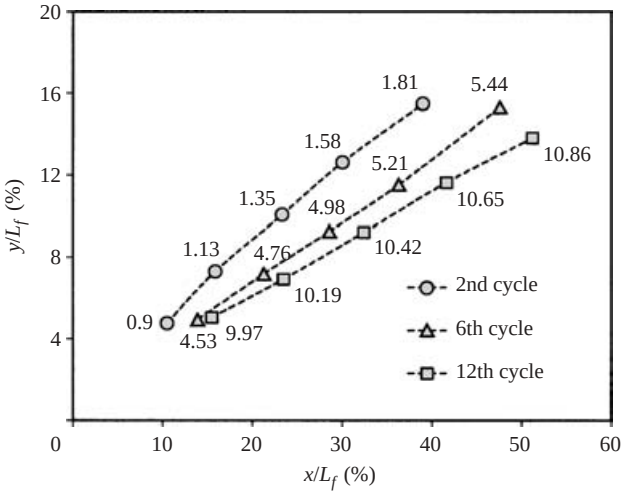

FIGURE 18. Vortex core location at different stages of reattachment; $Re_L = 1.44 \times 10^5$, $\Delta\alpha_r = 9^\circ$, $F^+ = 1.1$, $\langle c\mu \rangle = 0.06\%$.

corresponding phase-averaged surface pressures enabled some indirect gauging of the vortex dynamics. Accordingly, vortex convection speeds and their spatial amplification were investigated by analysing the surface pressure signatures. In order to resolve flow development during different stages of reattachment, the $\langle C_p \rangle$ time series obtained from each pressure tap were subdivided into segments. For each segment, the coherent constituent of the pressure coefficient, $\langle c_p \rangle_f = \langle C_p \rangle - C_p$, was Fourier transformed.

The average phase velocity, $\bar{u}_\phi$, of the fundamental mode derived from the Fourier decomposition of $\langle c_p \rangle_f$ was evaluated for the nth ($n = 1, 2, \ldots$) segment and prescribed location using the relation

$$\bar{u}_\phi(x, n) = 2\pi f \left(\frac{\Delta x}{\Delta \bar{\phi}(x, n)} \right), \tag{3.1}$$

where $\Delta\bar{\phi}$ is the phase difference between two adjacent pressure taps separated by a distance Δx. Cubic spline was used to smooth the data with respect to x.

Figure 19 represents the normalized phase velocities deduced from the pressure signature corresponding to the PIV measurements of figures 16 and 17 ($F^+ = 1.1$, $\langle c\mu \rangle = 0.06\%$, $\Delta\alpha = 9^\circ$). During the first two cycles of the excitation ($\tau < 1.8$), phase propagation is very slow near the flap shoulder reaching velocities as low as $\bar{u}_\phi / U_\infty = 0.15$ at $x/L_f \approx 5\%$. Farther downstream, the footprint of the passing vortices accelerates rapidly attaining a maximum $\bar{u}_\phi / U_\infty \approx 0.8$ ($x/L_f \approx 25\%$) before decelerating back to almost their initial speed ($x/L_f \approx 45\%$). The acceleration is then resumed, reaching $\bar{u}_\phi / U_\infty = 1$ at $x/L_f > 60\%$.

The amplitude of the spatial fluctuation in the phase velocity decreases with time and only a plateau, corresponding to $\bar{u}_\phi / U_\infty \approx 0.45$, is seen ($x/L_f \approx 45\%$) at times commensurate with the completion of reattachment. Actual vortex propagation speeds estimated from the phase-locked PIV data do not show as strong spatial accelerations as the pressure signatures, but they follow similar trends (figure 19 shows the velocities of four initial vortices). It is possible that the crude segmentation of the time series of $\langle c_P \rangle_f$ used to compute the Fourier coefficients introduced errors in the derivation of $\bar{u}_\phi / U_\infty$, especially during the initial stages when adequate phase information is not available everywhere along the flap.

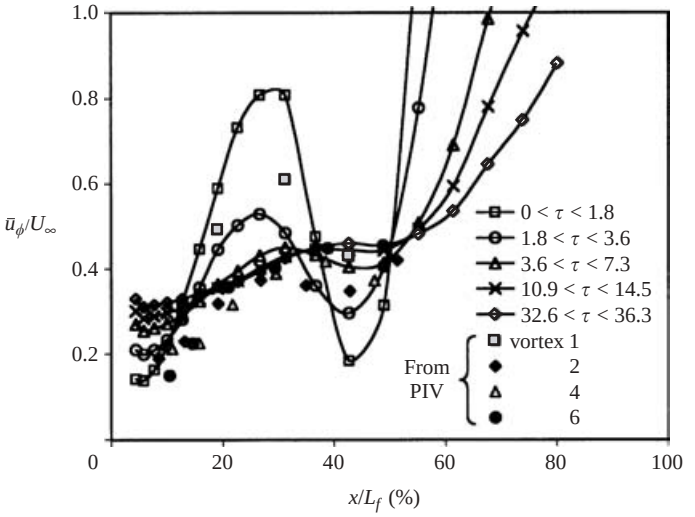

FIGURE 19. Phase velocities at different times during reattachment, computed from wall pressure and PIV data; $F^+ = 1.1$, $\langle c\mu \rangle = 0.06\%$, $\Delta\alpha = 9°$, $Re_L = 1.44 \times 10^5$.

The streamwise extent of the fluctuation and its intensity are strongly dependent on the frequency of the excitation. Doubling F^+, for example, halved the streamwise distance to the inflection point in $\bar{u}_\phi/U_\infty$ and increased the initial acceleration rates. Reducing the frequency to $F^+ = 0.6$ resulted in almost imperceptible time and space changes in the distribution of $\bar{u}_\phi/U_\infty$ (both cases are not shown).

Notwithstanding spatial fluctuations, the phase velocities averaged along the entire flap are $0.4 < \bar{u}_\phi/U_\infty < 0.5$ for all excitation frequencies and stages of reattachment. The corresponding dimensionless time required for a typical vortex to pass over the flap is $2 < \tau < 2.5$, which agrees with the rise time of the adverse surge in flap loading during the early stages of reattachment. The link between the flap offloading and the initial formation of the forced vortex gives a plausible reason for the independence of the surge duration from the reduced forcing frequency. It simply correlates with the advection speed of the initial vortex and not its size.

Amplitude distributions of the oscillatory wall pressure fluctuations $\langle c_p \rangle_f$ (corrected for system attenuations) at the same conditions and time intervals discussed above are shown in figure 20. Throughout the reattachment process, the spatial amplification of the pressure fluctuations is evident, followed by their decay. In addition, there is a gradual increase in the local amplitudes, as the process of reattachment progresses with time until a steady state is attained at large values of τ. In the case presented ($F^+ = 1.1$), the initial maximum amplitude ($Amp[\langle c_p \rangle_f] \approx 0.12$) had increased more than three-fold by the end of the process (and nearly doubled before $\tau = 7.3$). Concurrently, the location of the peak amplitude shifted from $x/L_f \approx 20\%$ to 30%. Similar temporal amplification ratios were observed at higher excitation frequencies, except that the streamwise distances corresponding to the location of these maxima were inversely dependent on F^+.

It is probable that the large temporal amplification during the initial stages of reattachment are caused by changes in the stability characteristics of the flow which are generally associated with the thinning of the boundary layer (see e.g. figure 13). Throughout the process, regions of intense flow reversal were observed near the surface at the fore part of the flap resulting in velocity ratio parameter $R > 1$ that at

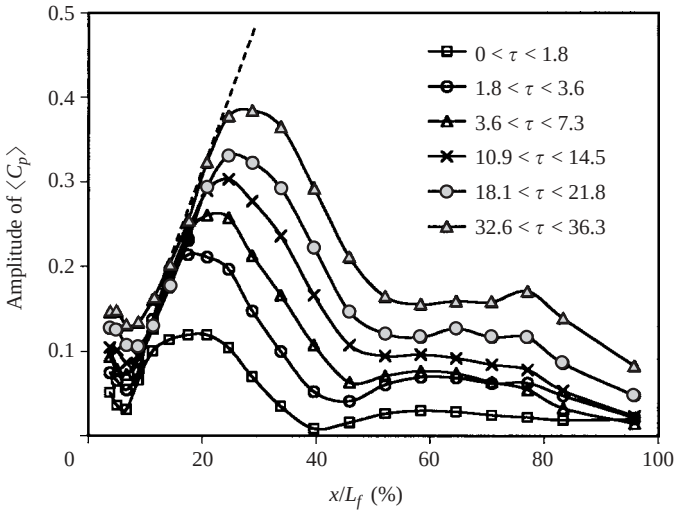

FIGURE 20. Amplitude distribution of wall pressure fluctuations during reattachment; $F^+ = 1.1$, $\langle c\mu \rangle = 0.06\%$, $\Delta\alpha = 9^\circ$, $Re_L = 1.44 \times 10^5$.

times was as high as 1.66. These values exceed the minimum criterion for absolute instability in a mixing layer between two streams, and there is reason to believe that they do so locally in the present flow. The existence of a limited region of absolute instability may also explain the very low eddy convection speeds near the flap shoulder and their subsequent acceleration further downstream.

Since the PIV data does not indicate strong intensification of the vortical structures during the course of reattachment, a question was raised as to whether the temporal increase in the amplitude of the pressure oscillations is, at least in part, a measure of the closeness of the eddies to the surface. This notion was rejected, however, because it does not support the constancy of the initial amplification rate of $\langle c_p \rangle_f$ (note the overlapping portions of the curves that are accentuated by the dashed straight line in figure 20). The contrast between the continual growth in the local pressure fluctuations and the apparent decay of the vortices observed in the PIV results at $x/L_f > 30\%$ (see figure 17), is mostly attributed to increased blurring of the ensemble-averaged structures owing random jitter in the phase-locked events.

In order to improve the correlation between the coherent constituents of the measured flow and the amplitude of the surface pressure fluctuations, a pattern-recognition technique has been formulated that reconstructs a more realistic manifestation of the average vortical structures (the details of the procedure are described by Darabi 2002). The merits of this vortex enhancement technique are illustrated in figure 21. It shows simply averaged phase-locked vorticity contours opposite their enhanced counterparts at two different times after the initiation of excitation (but relative to it at the same phase). In both cases, the reference window is retained to emphasize the increase in the advection velocity of the vortices with increasing time from the initiation of actuation. Comparison of the original and the enhanced structures reveals the extent of the distortion and blur resulting from simple phase averaging. The enhanced vorticity patterns are more regular and more intense, especially at later times of the reattachment. Their shape and size remains almost intact throughout the process.

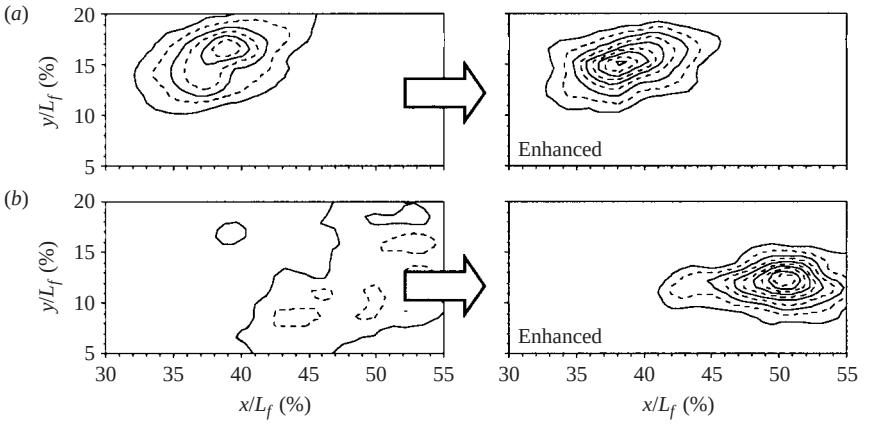

FIGURE 21. Simple and enhanced representation of like-phase vortical structures during reattachment. (*a*) $\tau = 1.8$, $t = 50$ ms, (*b*) $\tau = 10.6$, $t = 300$ ms.

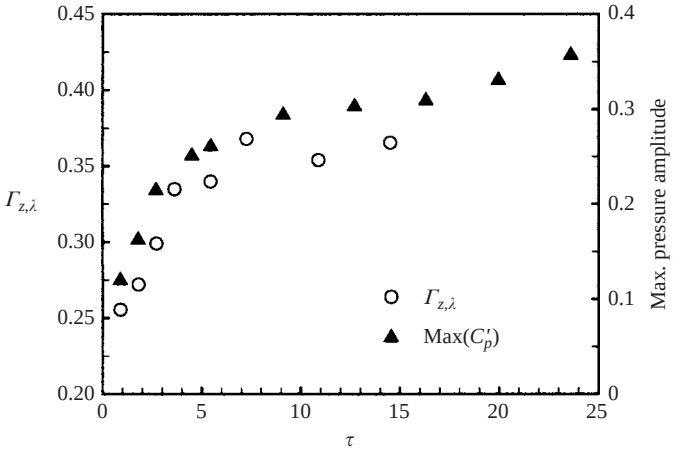

FIGURE 22. Time variation of the circulation within enhanced vortices (at constant phase) and of the peak pressure amplitudes; $Re_L = 1.44 \times 10^5$, $\Delta\alpha_r = 9°$, $F^+ = 1.1$, $\langle c\mu \rangle = 0.06\%$.

Figure 22 compares time variation in the spanwise circulation, $\Gamma_{z,\lambda}$, contained in the enhanced structures with that of the maximum pressure amplitudes in figure 20. The values of $\Gamma_{z,\lambda}$ were computed for structures at a constant phase relative to the excitation by spatial integration of the vorticity that exceeded some threshold level. There is clearly a good correlation between $\Gamma_{z,\lambda}$ and the pressure amplitudes during the initial stages of reattachment ($\tau < 7.2$), when both quantities amplify rapidly with τ. At later times, limitations imposed by the finite size of the PIV window made it impossible to calculate $\Gamma_{z,\lambda}$ accurately and the trend could not be verified for the entire duration of process.

3.4. *Vortex dispersion*

Figure 23 depicts contours of the quantity $\sqrt{u'^2 + v'^2}$ summing up the two components of the turbulent intensity, at two instants during reattachment – both measured at the same phase of the excitation. Evidently, most of the turbulent activity coincides with the location of the large vortices and it increases in significance as reattachment progresses. There is literally an order of magnitude difference between the turbulent

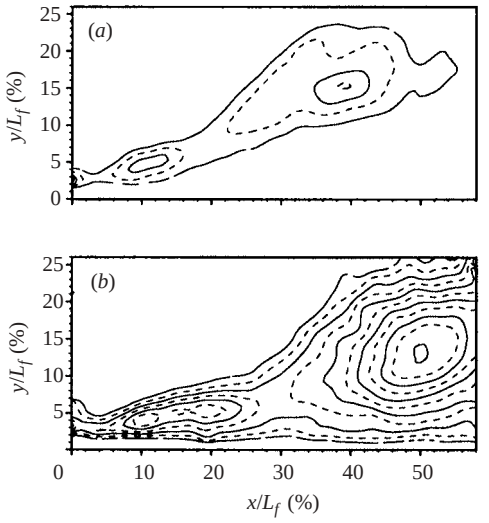

FIGURE 23. Two-dimensional distribution of the turbulent intensity ($\sqrt{u'^2 + v'^2}$) at two stages during reattachment; $Re_L = 1.44 \times 10^5$, $\Delta\alpha_r = 9°$, $F^+ = 1.1$, $\langle c\mu \rangle = 0.06\%$. (*a*) $\tau = 1.8$, $t = 50$ ms, (*b*) $\tau = 10.8$, $t = 300$ ms.

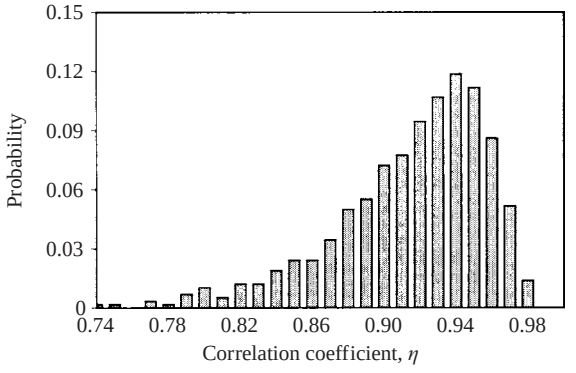

FIGURE 24. Probability distribution of the two-dimensional correlation between individual vortices and the enhanced average vortex; $\Delta\alpha_r = 9°$, $F^+ = 1.1$, $\langle c\mu \rangle = 0.06\%$, $\tau = 5.44$.

energies associated with the initial vortex occurring at $\tau = 1.8$ and that at $\tau = 10.8$. Since, as demonstrated above, a typical eddy does not change much in size and shape, the apparent increase in the turbulence content indicates growing jitter in vortex locations at a given phase.

The extent of this random meandering of the vortices could be straightforwardly examined by using information generated as part of the enhancement procedure. The process yielded two distinct variables: (i) the correlation coefficient η_i, expressing the degree of resemblance of the ith realization to the enhanced average vortex; (ii) the vector $\Delta X_i = (\Delta x_i, \Delta y_i)$, representing the displacement of the core of the ith vortex (determined by the location of the maximum correlation) relative to the enhanced average vortex. Figure 24 presents a typical probability distribution of η_i based on a relatively large number (570) of events corresponding to the dominant vortex observed at $\tau = 5.4$ (centred at $y/L_f \approx 15\%$, $x/L_f \approx 48\%$; see figure 17).

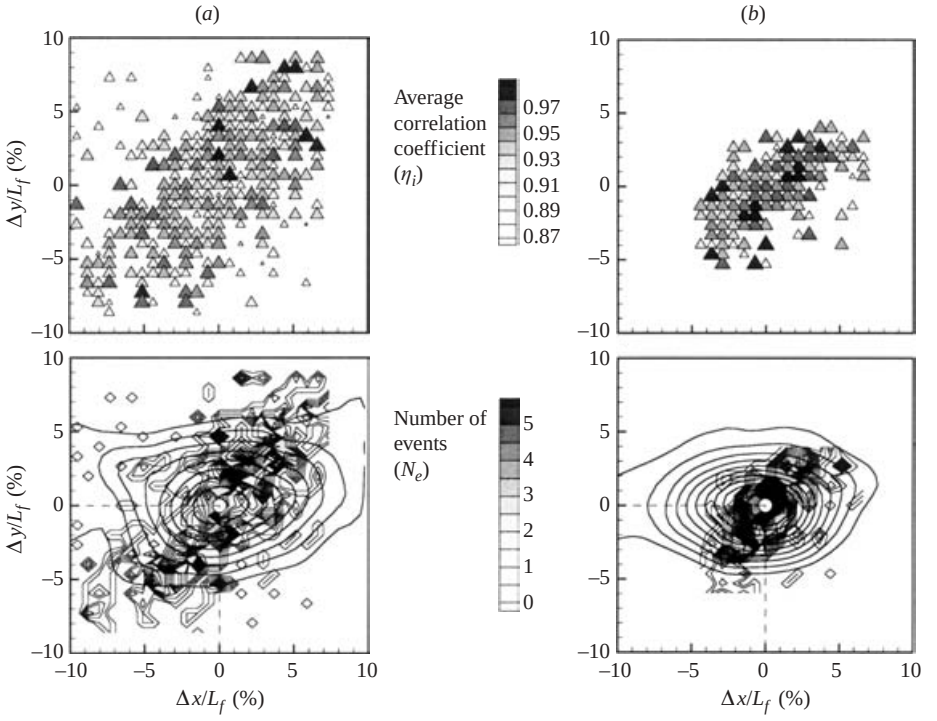

FIGURE 25. Two-dimensional distribution of the correlation coefficient, η_i, and number distribution. (*a*) $\tau = 5.44$ ($\Phi = 2\pi$), (*b*) $\tau = 4.99$ ($\Phi = \pi$).

When the locations ΔX_i of the highest correlation are to be displayed together with the η_i data, the result is a two-dimensional scatter plot, as the one shown in figure 25(*a*) (top). Each value of η, differentiated by both symbol size and grey level in this plot, represents a local average correlation; namely, it is the product of all the events having the same ΔX_i. Figure 25(*a*) (bottom) complements this data by overlaying the two-dimensional number distribution of the events N_e with isodynes representing the enhanced vortex. Together, these two plots demonstrate the following dispersion characteristics for the current time step:

(i) There is no apparent preference or correlation between the locations of the vortex population and their degree of coherence.

(ii) The data seems to be distributed elliptically along an inclined axis, oriented at about 45° relative to the flap surface (∼20° relative to the mean flow). This slope indicates that vortices that are located further from the flap surface travel faster than their counterparts near the surface.

(iii) The variance of the lateral vortex displacements $\Delta y'$ is large. It is about twice the width of the longitudinal displacements $\Delta x'$ and it is comparable to the local distance between the vortices and the surface.

Similar data taken half a forcing cycle earlier ($\tau = 4.99$) are shown in figure 25(*b*). At this stage, the vortex is located closer to the flap shoulder. Although scatter is reduced at the earlier phase, the ratio $\Delta x'/\Delta y'$ and the inclination angle of the data dispersal are comparable at both times. Apparently, the correlation levels decrease with increasing time and distance from the origin while the extent of vortex dispersion ($\Delta x', \Delta y'$) increases.

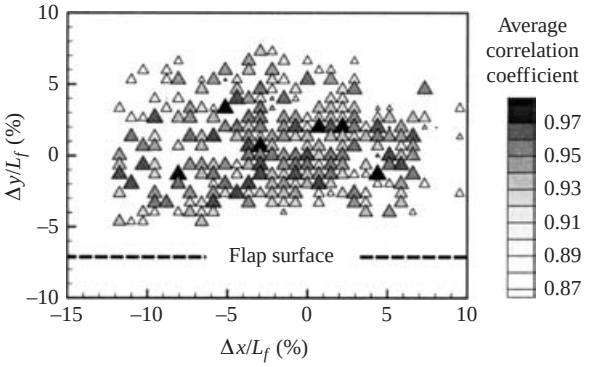

FIGURE 26. Two-dimensional distribution of the correlation coefficient, η_i, at the end of the reattachment; $Re_L = 1.44 \times 10^5$, $\Delta\alpha_r = 9°$, $F^+ = 1.1$, $\langle c\mu \rangle = 0.06\%$.

When a similar analysis is applied to other stages of reattachment while maintaining the same two phases, the following conclusions are drawn:

(i) The coherence of vortex realizations at a fixed phase deteriorates as reattachment progresses.

(ii) The extent of the spatial dispersion at a fixed phase increases until it becomes comparable with the distance between the vortex and the surface. This point is presumably reached during the initial stage ($\tau < 5.4$).

(iii) As the mean vortex approaches the flap surface, the variance of the streamwise displacement $\Delta x'$ gradually surpasses $\Delta y'$. Upon completion of reattachment (figure 26), the ratio $\Delta x'/\Delta y'$ equals approximately two (i.e. the inverse of the initial ratio).

The spatial increase in vortex meander during reattachment may have an influence on the perceived wall pressure fluctuations, particularly on the decay seen in the amplitudes downstream of $x/L_f \approx 30\%$ (figure 20). As the jitter level in structure positions becomes comparable with their wavelength, random shifts in the phase-locked signals can result in amplitude attenuation at the fundamental frequency – even if the strength of the structures does not change. This notion is supported by the fact that there is no apparent drop in the size or intensity of the (enhanced) vortices downstream of $x/L_f = 30\%$. It should be noted that the circulation values presented in figure 22 are computed for vortices located at $35\% < x/L_f < 55\%$, but they are compared with the maximum pressure amplitudes which are further upstream. Thus, it is reasonable to assume that vortex intensity is approximately maintained even beyond the amplification zone in figure 20.

3.5. *Vortex activity*

The beneficial role of the organized vortices in promoting flow reattachment was evaluated using the phase-locked PIV data. In most cases, the PIV captured two adjacent structures within the measurement window, which made it possible to extract the velocities normal to the axis connecting them and establish the volume-flow-rate q_e crossing between their cores (figure 27). Calculations of q_e were applied to data corresponding to two phases (arbitrarily denoted 0 and $\frac{1}{2}\pi$), at different stages of reattachment.

Volume flux computed from regular ensemble-averaged PIV data, as well as enhanced data, is plotted in figure 28. The results are normalized by the amplitude of the oscillatory jet flow at the slot exit, $\langle q_j \rangle = g\langle u_j \rangle$ (where $\langle u_j \rangle$ is the jet velocity

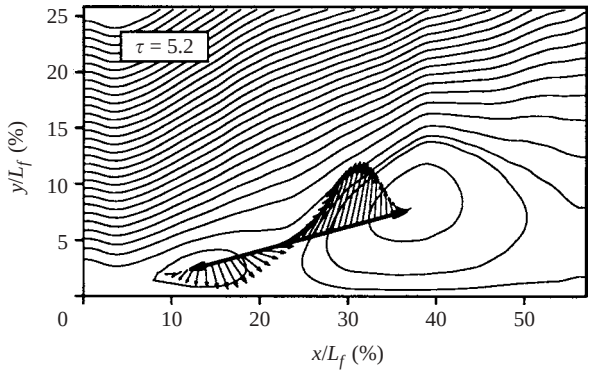

FIGURE 27. An illustration of the phase-locked velocities along the axis connecting two adjacent vortex cores.

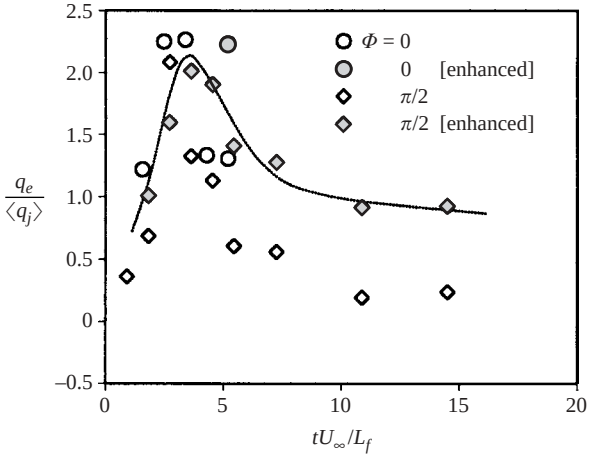

FIGURE 28. The net flow crossing between two adjacent vortex cores as a function of τ, at two phases during reattachment.

amplitude and g is the slot height). In all cases tested, the relative entrainment $q_e/\langle q_j \rangle$ is positive, i.e. pointing away from the wall. The relative entrainment peaks at almost 2.5 around $\tau = 4$ and then decreases to values of nearly unity during the advanced stages of reattachment. The positive values of the entrainment are attributed to the fact that the downstream vortex always induces outward flow that exceeds, in absolute terms, the opposed flow by the upstream vortex. This ties in directly to the size differences between the two structures owing to the spatial amplification that they undergo. We may conclude that arrays of vortices in the perturbed flow generate a net outward transport of mass and momentum across the shear layer as they travel downstream. This vortex activity is limited to regions where the vortices are being amplified, spatially, and it presumably ceases beyond the point of neutral amplification. The vortices in this region may be regarded as moving pumps. They constantly draw fluid from the dwindling reservoir of fluid available for entrainment near the surface of the flap, consequently lowering the local static pressure. The resulting favorable pressure gradient forces the mean flow to reattach. Since it typically takes about one wavelength for small perturbations in a mixing layer to reach the neutral amplification point, it is easy to understand why reduced

excitation frequencies of $O(1)$ perform best in controlling flow separation (when the length scale in the reduced frequency is based on the length of the separated region).

4. Summary

It was demonstrated that the parameters $\Delta\alpha$, $\langle c\mu \rangle$ and F^+ that control the stationary flow over a highly deflected flap also regulate the duration of the reattachment process. Minimum reattachment time, $\tau_{r,min} \approx 16$, is achieved at $\Delta\alpha_r = 6^\circ$ when the flow is excited at an optimal frequency of $F^+_{opt} \approx 1.5$ and at high amplitudes. The effect of the amplitude saturates above $\langle c\mu \rangle \approx 0.1\%$. The load on the flap increases almost linearly with time ($F^+ > 1$) except during the early stages of the reattachment process ($0 < \tau < 5$), when a short-lived force is generated in the opposite direction (the flap is actually being offloaded). The duration of this adverse surge is independent of the frequency of excitation and of $\Delta\alpha$. Its appearance is directly related to the propagation of the initial vortex generated by the excitation that induces intensive pressure rise ahead (downstream) of itself. The duration of the surge is determined by the convection speed of the first vortex along the flap.

The key feature enabling the reattachment is the generation of organized structures in the flow. It was observed that the amplification of the perturbations in the shear layer vary in space and in time during forced reattachment, stretching and thinning it at the same time. The emerging vortices attain higher amplitudes and they preserve their strength farther downstream at later stages of the process. Close to the flap shoulder ($x/L_f < 20\%$), the flow is probably absolutely unstable during most of the reattachment process, enabling strong temporal amplification of global modes. At the end of the process, the same region is only convectively unstable permitting spatial amplification of the imposed excitation. The global instability may also result in a very low initial convection speed of the eddies.

It was shown that the forced reattachment of the flow could be attributed to the enhanced entrainment caused by passage of the organized vortices. Vortex activity throughout the amplification zone results in a net outward transport of mass across the shear layer that lowers the static pressure near the surface of the flap. The ensuing transverse pressure gradient then forces the mean flow to reattach to the surface. Since the deflection of the main stream is not immediate, the effectiveness of the excitation is attributed to the disparity in the time scales between the period of the imposed oscillations and the time required to accomplish the reattachment process.

The authors would like to thank Professor L. Lourenco for his help in setting up the PIV system and his useful suggestions about the various aspects of this new and powerful experimental tool.

REFERENCES

Ahmed, N. A. & Wagner, D. J. 2003 Vortex shedding and transition frequencies associated with flow around a circular cylinder. *AIAA J.* **41**, 542.

Amitay, M., Smith, B. L. & Glezer, A. 1998 Aerodynamic flow control using synthetic jet technology. *36th Aerospace Sciences Meeting and Exhibit, Reno, NV*, *AIAA Paper* 98-0208.

Béra, J. C., Michard, M., Sunyach, M. & Comte-Bellot, G. 2000 Changing lift and drag by jet oscillation: experiments on a cylinder with turbulent separation. *Eur. J. Mech.* B *Fluids*, 1–21.

Collins, F. G. & Zelenevitz, J. 1975 Influence of sound upon separated flow over Wings. *AIAA J.* **13**, 408–410.

Darabi, A. 2002 On the mechanisms of forced flow reattachment. PhD Thesis, Tel-Aviv University.

Darabi, A. & Wygnanski, I. 2004 Active management of naturally separated flow over a solid surface. Part 2. The separation process. *J. Fluid Mech.* **510**, 131–144.

Greenblatt, D. & Wygnanski, I. 2001 The control of flow separation by periodic excitation. *Prog. Aerospace Sci.* **36**, 487–545.

Grife, R., Darabi, A. & Wygnanski, I. 2002 Download reduction on a three dimensional V-22 model using active flow control. *1st Flow Control Conf. St Louis, MO*, *AIAA Paper* 2000-3071.

Huerre, P. & Monkewitz, P. A. 1990 Local and global instabilities in spatially developing flows. *Annu. Rev. Fluid Mech.* **22**, 473–537.

Katz, Y., Nishri, B. & Wygnanski, I. 1989 The delay of turbulent boundary layer separation by oscillatory active control. *AIAA Paper* 89-0975 also *Phys. Fluids* A **1**, 179–181.

Naim, A. 2003 Active control of cylinder flow with and without a splitter plate. MSc thesis, Tel-Aviv University.

Nishri, B. & Wygnanski, I. 1998 Effects of periodic excitation on turbulent flow separation from a flap. *AIAA J.* **36** 547–556.

Nishri, B. 1995 On the dominant mechanism of active control of flow separation. PhD thesis, Tel-Aviv University.

Oster, D. & Wygnanski, I. 1982 The forced mixing layer between parallel streams. *J. Fluid Mech.* **123**, 91–130.

Seifert, A., Darabi, A. & Wygnanski, I. 1996 Delay of airfoil stall by periodic excitation. *AIAA J. Aircraft* **33**, 691–698.

Seifert, A., Bachar, T., Koss, D., Shepshelovich, M. & Wygnanski, I. 1993 Oscillatory blowing: a tool to delay boundary-layer separation. *AIAA J.* **34**, 2052–2060.

Taubert, L., Kjellgren, P. & Wygnanski, I. 2002 Generic bluff bodies with undetermined separation location. *1st Flow Control Conf. St Louis, MO*, *AIAA Paper* 2002-3068.